The Missing Link for Electrochemical CO_2 Reduction: Classification of CO vs. HCOOH Selectivity via PCA, Reaction Pathways and Coverage Analysis

Oliver Christensen,[†] Alexander Bagger,[‡] and Jan Rossmeisl[*,†]

[†]*Department of Chemistry, University of Copenhagen, Universitetsparken 5, Copenhagen, Denmark*

[‡]*Department of Physics, Danish Technical University, Fysikvej, Kgs. Lyngby, Denmark*

E-mail: jan.rossmeisl@chem.ku.dk

Abstract

For the electrochemical CO_2 reduction reaction, different metal catalysts produce different products preferentially. However, the differences between the metals' reaction pathways that lead to these different products is still not fully understood. In this work, we analyze CO vs. HCOOH formation from CO_2 using statistical analysis and DFT calculations. This is carried out by considering multiple descriptors, along with the competing reaction pathways, reaction barriers, and high coverage of mixed adsorbates on the surface. This method is capable of explaining the discrepancy between simulations and experiments regarding Ag and Au selectivity, and of properly classifying elements according to their product distribution. We find that, when considering water-assisted protonation for the disproportionation to CO, Ag and Au have a lower barrier for CO production in agreement with experimental results. We also find

that, when considering high coverage of mixed adsorbates on the Ag/Au surface, the most stable adsorbate configuration contains adsorbates capable of forming CO preferentially. These findings help to bridge the gap between simulations and experiments and provide a missing link for our understanding of the CO_2 reduction reaction.

1 Introduction

Due to pollution, climate change, and the need to store and produce renewable energy sustainably and effectively, there is an acute need for CO_2 utilization methods such as electrochemical CO_2 reduction (CO_2R).[1–6] As a result of this, scientific and industrial interest in CO_2R has increased greatly over the last few decades. The CO_2 reduction reaction (CO_2RR) is complex, in large part due to the many different products and reaction pathways.[1,7,8] To achieve performance good enough for industrial applications, however, understanding and tuning the CO_2RR to give specific products with high enough selectivity and activity is essential.

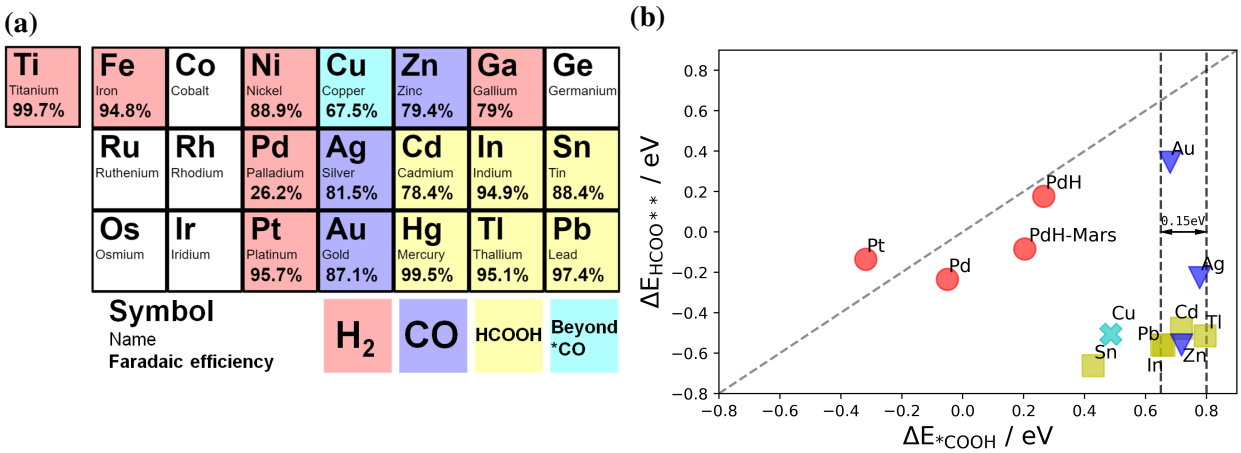

Figure 1: **(a)** Major product classification of metal catalysts for CO_2 electroreduction based on the experiments of Hori et al.,[9] colored according to major product selectivity. **(b)** Calculated adsorption energies for ΔE_{*COOH} vs. ΔE_{HCOO**} for different metal catalysts.

One of the main challenges here is finding out why different catalysts give different products.[10,11] Previous work by Hori et al.[9] grouped the transition metals according to whether they produce mainly H_2 (Ti, Fe, Ni, Pd, Pt, Ga),[12] CO (Ag, Au, Zn),[13–18] HCOOH (Cd, In, Sn, Hg, Tl, Pb),[19–21] or hydrocarbons and alcohols, here denoted as *beyond *CO* (Cu).[22–27] Fig. 1a shows the

grouping of the metal catalysts according to their major product, with the assigned color and the Faradaic efficiency for the major product shown for each metal.[23,28] The colors given for the four groups in Fig. 1 are utilized throughout the work to show the product classification. We previously found descriptors explaining the selectivity of Cu and H_2-producing metal catalysts in the binding energies of ΔE_{*H} and ΔE_{*CO}.[28] However, neither the observed relation of ΔE_{*H}, nor the analysis of anyone else to our knowledge, fully provides an empirically based explanation of why different metals give different products.

This discrepancy between experimental and simulational results for the CO_2RR has also been noted by Bohra et al.[29] In likely the most egregious example, we know experimentally that Ag and Au produce CO.[23] However, Density Functional Theory (DFT) calculations predicts that the formation of HCOOH has a lower barrier compared to CO, meaning that these elements preferentially produce HCOOH, in disagreement with experimental knowledge.[11,29] As DFT is generally very good at qualitatively predicting (electro)catalytic trends in agreement with experiments,[2] there must be some factor that has not yet been accounted for in atomic-scale simulations.

A popular assumption in the field of electrochemical CO_2 reduction is that the monodentate intermediate *COOH produces CO, while the bidentate intermediate HCOO** produces HCOOH (see Fig. 2 for illustration of adsorbates).[29,30] The reasoning then goes, if one can show the existence or stability of the given intermediate, one has proven product formation of its assumed corresponding product. Unfortunately, there are problems with this thinking. Fig. 1b shows the DFT adsorption energies of *COOH vs. HCOO** for several metal catalysts. The diagonal dashed line indicates the points where the two adsorption energies are equal, while the vertical dashed lines indicate how similarly CO-producing (blue) and HCOOH-producing (yellow) metals bind *COOH, being within simulation margin of error energy-wise. With the exception of the H_2-producing Pt, every other metal preferentially binds the intermediate HCOO** over *COOH, i.e. are below the diagonal line. Meaning, according to DFT, Ag and Au should have mainly HCOO** on the surface, and thus mainly produce HCOOH. But if that is the case, how do they make CO? In other words, we need to expand our theoretical framework to explain this phenomenon.

Several studies have tried to give an explanation regarding CO vs. HCOOH selectivity.[10,11,17,28–42] Many hypotheses have been made as to what critical factor is needed to consider in order for theoretical calculations to explain this part of CO_2R product selectivity, such as pH, cations, the surface structure, the amount of water molecules in solution, the binding energy and coverage of protons on the surface, steric constraints, and adsorbate-adsorbate interactions. So far, however, a comprehensive, data-based explanation, reproducing the experimental trends with DFT calculations and explaining CO vs. HCOOH selectivity, has to our knowledge not been made.

The aim of this paper is to investigate the distinction between CO- and HCOOH-producing metal catalysts. This work differs from previous research in the field in four significant ways:

- This work investigates a multitude of different descriptors and metals, using statistical analysis to understand the descriptor space.
- This work investigates both the CO and HCOOH pathways simultaneously for direct comparison, on a wide variety of metal surfaces.
- This work investigates not only the adsorption energies, but also the related activation energies for the proposed rate- and/or product-determining steps of the reaction (see Eq. 3-7).
- This work considers everything from a single adsorbate to full coverage of the surface, for all investigated adsorbate combinations. Some recent studies have looked into higher coverage of adsorbates,[30,32] but do not mix different adsorbates on the surface.

We posit that these factors can qualitatively explain the selectivity difference between CO- and HCOOH-producing elements. By themselves, none of these features are entirely new, but have often been overlooked or used sparingly due to the difficulty and resource intensity in calculating transition states and high-coverage structures for so many different features and elements. Combining these approaches through thorough theoretical investigation of the CO_2RR, we hope to find new insight for CO_2RR and especially CO vs. HCOOH selectivity on the different metal catalysts.

2 Descriptors and Pathways Investigated

For this work, we investigated a wealth descriptors, including adsorption energies of various relevant adsorbates, reaction barriers for several competing reaction pathways, and physical descriptors such as the lattice constant (LC) and slab work function (WF) for several metal catalysts. The full list of descriptors used for the statistical analysis can be found in Fig. S2.

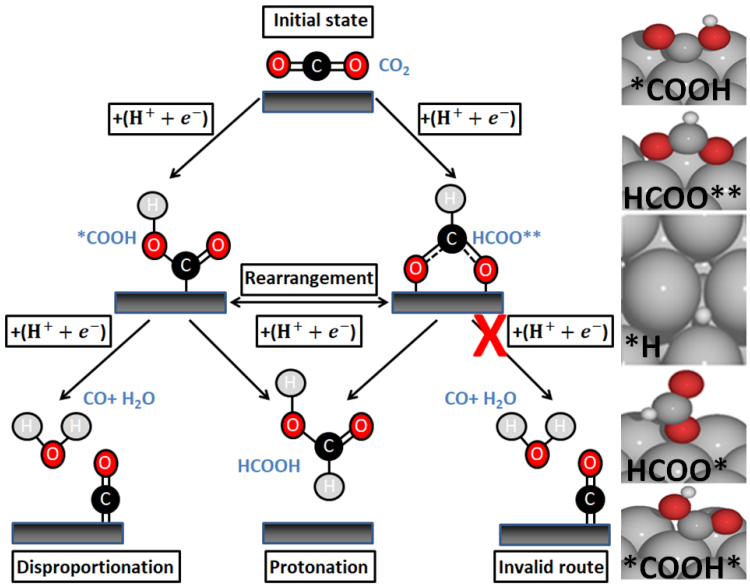

Figure 2: Left: Scheme for the CO_2R reaction pathways for CO and HCOOH formation. Conversion to CO occurs via a disproportionation reaction, while conversion to HCOOH occurs via protonation. Note that monodentate HCOO* is metastable but can exist when walled in by other adsorbates.[35] Right: Atomic visualizations of investigated intermediates for CO/HCOOH formation.

Fig. 2 shows the investigated reaction scheme for CO_2 reduction to either CO or HCOOH, which occurs via two proton-coupled electron transfer (PCET) reactions. Atomic visualizations of the intermediates are shown to the right. The first PCET is the conversion of CO_2 to one of the competing intermediates, either *COOH (Eq. 1) or HCOO** (Eq. 2), the activation step:

$$CO_2(g) + *H \rightarrow *COOH \quad (1)$$

$$CO_2(g) + *H \rightarrow HCOO** \quad (2)$$

These intermediates can then either form CO and H_2O via a disproportionation reaction (3 and 5), or HCOOH via protonation (4 and 6), the desorption step:

$$*COOH + *H \rightarrow H_2O(g) + CO(g) \quad (3)$$

$$*COOH + *H \rightarrow HCOOH(g) \quad (4)$$

$$HCOO** + *H \rightarrow H_2O(g) + CO(g) \quad (5)$$

$$HCOO** + *H \rightarrow HCOOH(g) \quad (6)$$

$$2*COOH \rightarrow H_2CO_3(g) + CO(g) \quad (7)$$

Pathway 7 was investigated as an alternative CO-producing pathway with carbonic acid (H_2CO_3) as a side product. Monodentate, metastable HCOO* has similar reaction pathways to *COOH and was also investigated as an alternate CO-producing intermediate.

3 Part 1: Statistical Insight

We would like to note that our goal is not to model CO or HCOOH, nor a specific reaction mechanism. Rather, the objective of this analysis is to discover what surface properties of the metal describe and determine CO_2RR product selectivity. Testing the multitude of descriptors described in the section above left us with a substantial dataset. We then applied Principal Component Analysis (PCA) to our dataset, in order to find the grouping of metal catalysts according to their major product selectivity.[43] PCA allows us to perform dimensionality reduction on our dataset while still explaining and retaining most of the information and variance in our dataset. However, PCA gen-

erally does not do well with missing data points. For this reason, it was decided only to do the analysis for 11 different elements and 22 different features.

Fig. 3 shows a 3D plot of PC#1 vs. PC#2 vs. PC#3 (Fig. 3a), along with corresponding 2D subplots for PC#1 vs. PC#2 (Fig. 3b), PC#1 vs. PC#3 (Fig. 3c), and PC#2 vs. PC#3 (Fig. 3d). Select original features used to make the PCA are projected onto PCA space in black. We observe that all the metals are nicely grouped according to their main product color. Note especially the separation between the CO- (blue) and HCOOH-producing (yellow) metals, which previous descriptor plots were unable to fully separate.[10,11,17,28–42] All 4 PCA plots describe 70+% of the variation in the dataset (additional PCA plots and discussion can be found in the SI section "*Additional PCA Results*".). This is a strong indicator that a 2D and 3D representation of metal catalyst product distribution is suitable. Note that simply using a 2D descriptor plot with PC#1 vs. PC#3 still manages to fully separate the elements according to their major product, although the distance between CO- and HCOOH-producing metals is smaller. As we use principal components rather than individual descriptors, this plot does not directly tell us which of the features in the dataset are the most important for understanding CO_2RR selectivity. We cannot translate our PCA statistical insight directly to chemical insight in the form of a reaction mechanism, although our results do give us additional mechanistic insight.

However, this analysis is based on the hypothesis that something in the metal catalyst surface decides or describes the selectivity, and of course the features we have chosen (DFT adsorption energies, WF, LC) are directly connected to the surface. Thus, the fact that we can separate the elements according to their product distribution this nicely using only the given simple descriptors, strongly supports this hypothesis regarding the deciding factor of the catalyst surface.

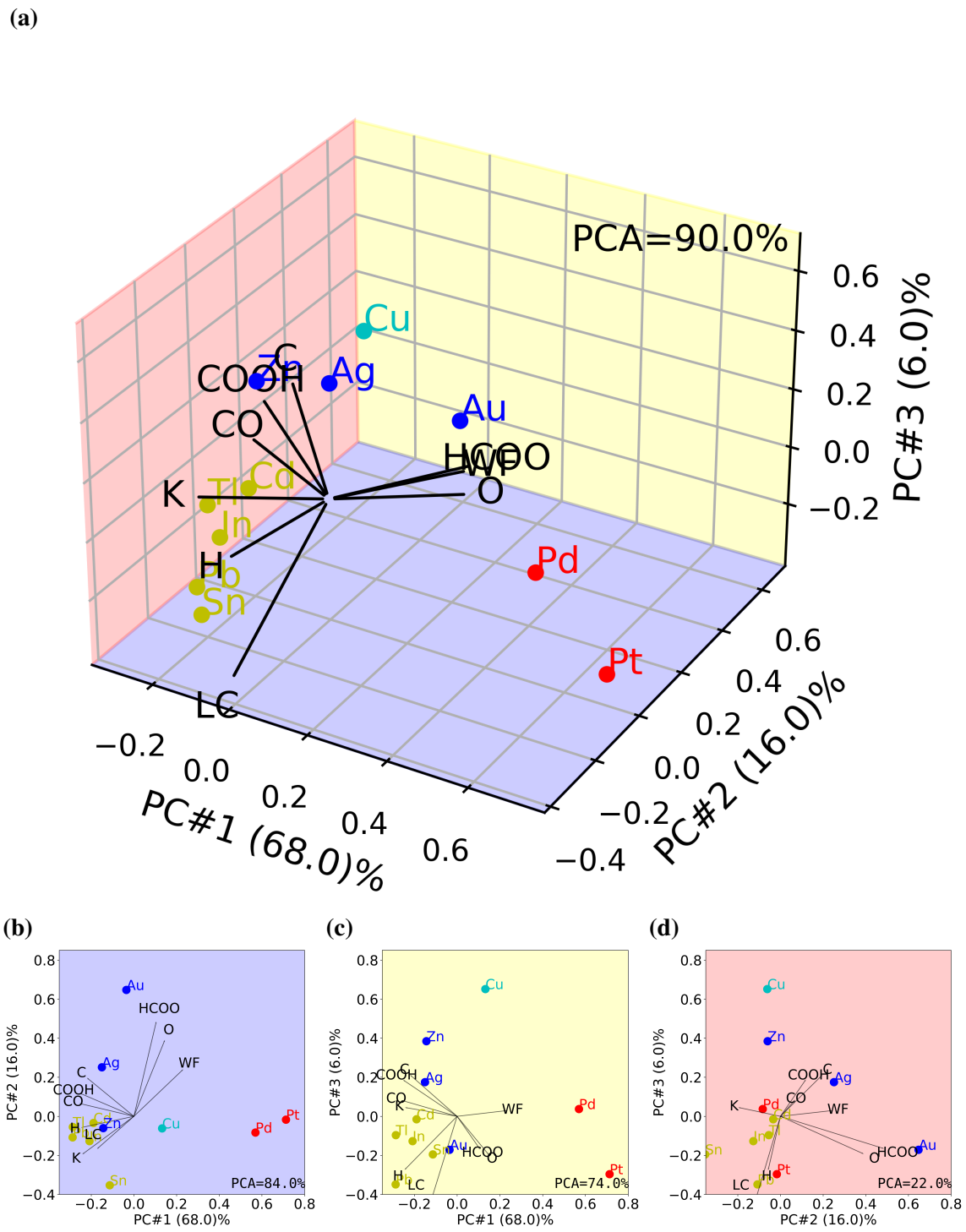

Figure 3: (**a**) PCA plots for PC#1 vs. PC#2 vs. PC#3, with projections of select original features (black), (**b-d**) along with corresponding 2D subplots. The PCA explained variance from the plotted principal components is plotted to show how much of the variance the plotted components describe. Metal catalysts are colored in accordance with their major product selectivity as shown in Fig. 1a, and each background plane in (**a**) is colored to match the 2D projections in (**b-d**). The projection of select original are coplotted in black on the PCA plot.

3.1 Basic Descriptors Classify CO_2RR Metal Catalysts

We can use the PCA, along with the projected features, to get information about which features are important for grouping the elements according to product selectivity. We observe from Fig. 3 that *H and LC group with the HCOOH-producing metals (yellow), while *CO, *C, and *COOH group with the CO-producing metals (blue), and *O, WF and HCOO** groups more closely with the H_2-producing metals (red). Especially LC seems to be an important feature for the PCA based on the length of the vector. Previous work has shown that using *CO and *H as descriptors is able to separate Cu, H_2- and CO_2RR-producing metals, but failing in separating CO- and HCOOH-producing metals.[28] Fig. 4 shows a 3D plot of *H vs. *CO vs. LC (Fig. 4a), along with corresponding 2D subplots for *H vs. CO (Fig. 4b), *H vs. LC (Fig. 4c), and LC vs. *CO (Fig. 4d). Note that this plot contains additional metal catalysts compared to Fig. 3, as not all elements investigated had data for all the required 22 features to be part of the PCA. Despite being based on 19 fewer features than the PCA and only requiring simple adsorbate calculations, the 3D plot (Fig. 4a), as well as the 2D plots of *H vs. LC and *CO vs. LC (Fig. 4c-d) group the elements just as well if not better than the PCA. To our knowledge, Fig. 4 is the best descriptor plot for CO_2RR product selectivities, and the first one to fully separate the different elements according to their main product. We already know that $\Delta E_{*\mathrm{H}}$ decides whether a metal has hydrogen underpotential deposition (H_{UPD}), while $\Delta E_{*\mathrm{CO}}$ seems to decide whether a metal does mainly HER or CO_2RR.[28] The question is what new insight the lattice constant as a descriptor gives us, seeing as how it clearly separates CO- and HCOOH-producing metals.

This seems related to geometry and how the adsorbates sit on the surface. Fig. S13 shows how HCOO** sits on metal surfaces with a small LC [ex. Au(111)] vs. metal surfaces with a large LC [ex. Pb(111)]. On Au(111) and other CO-producing metals, HCOO** sits inflexibly, with each *O on a separate ontop site. If two neighboring ontop sites are not available in a given area on the surface, bidentate cannot adsorp, instead making room for monodentate adsorbates like *COOH (see below for further discussion of this). On Pb and other HCOOH-producing metals, the distance

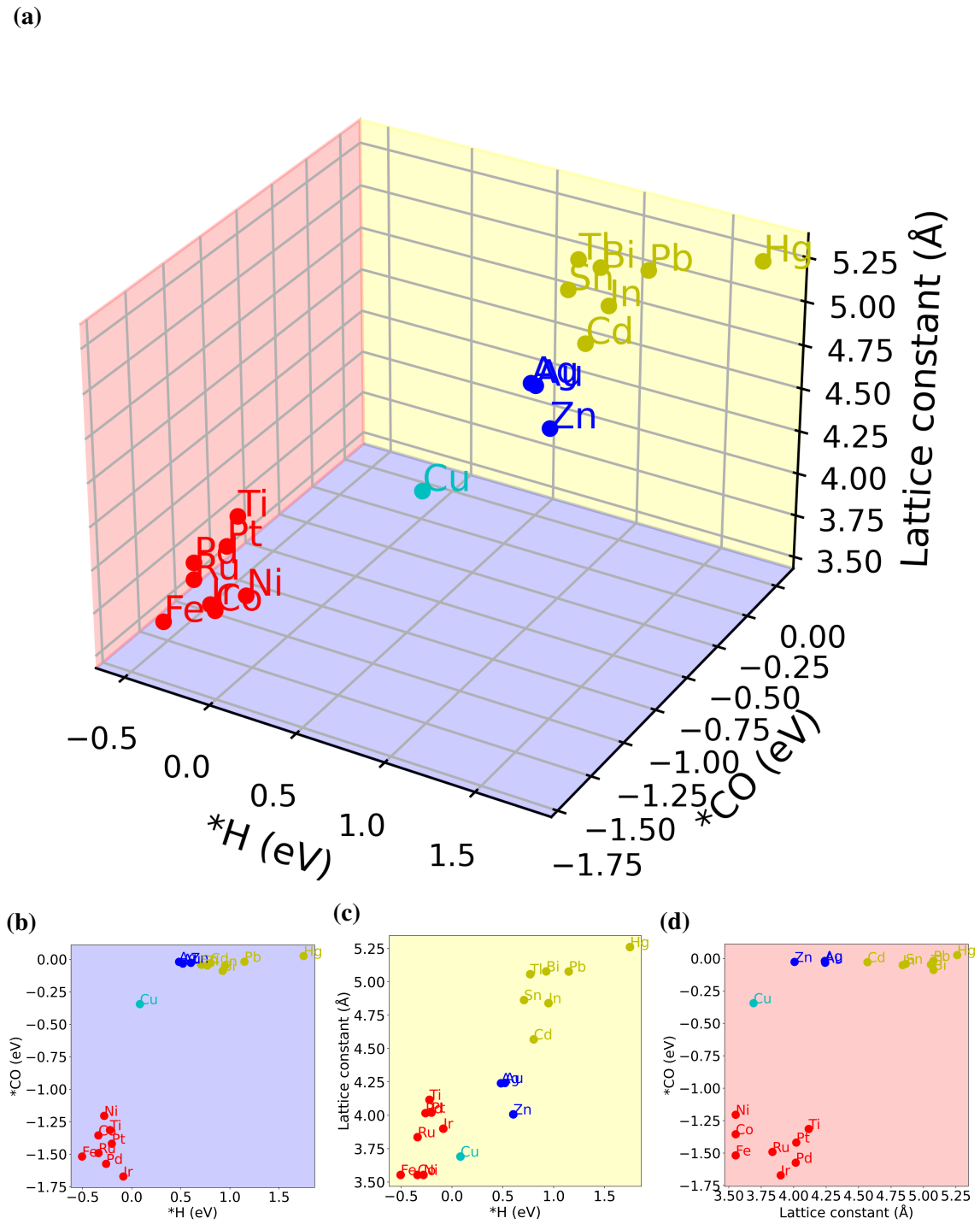

Figure 4: (**a**) Descriptor plot for lattice constant (LC) vs. adsorption energy of *H vs. adsorption energy of *CO, (**b-d**) along with corresponding 2D subplots. Metal catalysts are colored in accordance with their major product selectivity as shown in Fig. 1a, and each background plane in (**a**) is colored to match the 2D projections in (**b-d**).

between two ontop sites is too big. HCOO** instead sits in a saddle position on a single ontop site. This means that the coverage of HCOO** is more liquid, and it may be easier for it to fill the available space on the surface, leaving no room for something like *COOH.

One thing to consider about our descriptor model is whether it truly is predictive. For that reason, we calculated the descriptor values for metallic Bi, which was recently shown experimentally by Yang et al. to produce HCOOH with 90+% selectivity (see Fig. 4).[44] We find that Bi agrees fully with the 3 chosen descriptors, grouping together smack in the middle of the other HCOOH-producing (yellow) elements. This supports the predictive power of our model.

In summary, this simple descriptor plot allows us to group all the metals correctly according to their main product selectivity. However, it still leaves open the question of the exact mechanism for why Ag and Au produce CO, and Pb and Bi produce HCOOH.

4 Part 2: Derived Mechanistic Insight

4.1 CO Formation Most Likely Pathway From Monodentate *COOH/HCOO*

As part of our investigation, we calculated the activation energies for all the pathways in Eq. 1-7 for a dozen metal catalysts. In addition to vacuum DFT calculations, some or all of these pathways were investigated with different simulation setups, such as: different amounts of *H monolayer (ML), spectator adsorbates, or implicit addition of solvent (see SI section "*Additional Transition State Results*"). However, we found no clear answer to the discrepancy between simulations and experiments for Ag and Au when considering just surface-bound *H as the proton source. These results showed HCOO** to form more readily than *COOH from CO_2 for CO-producing Ag and Au, and also for HCOOH to form more readily than CO, regardless of the intermediate adsorbate. For further discussion of these results, see SI Section "*Direct Reaction Pathway Results*".

Research by Morrison et al. and Tang et al. has hypothesized that selectivity for CO vs. HCOOH can be determined by the amount of *H available, and whether the reaction proceeds via a Tafel or Heyrovsky mechanism.[30,39] While this hypothesis does not explain the preferential

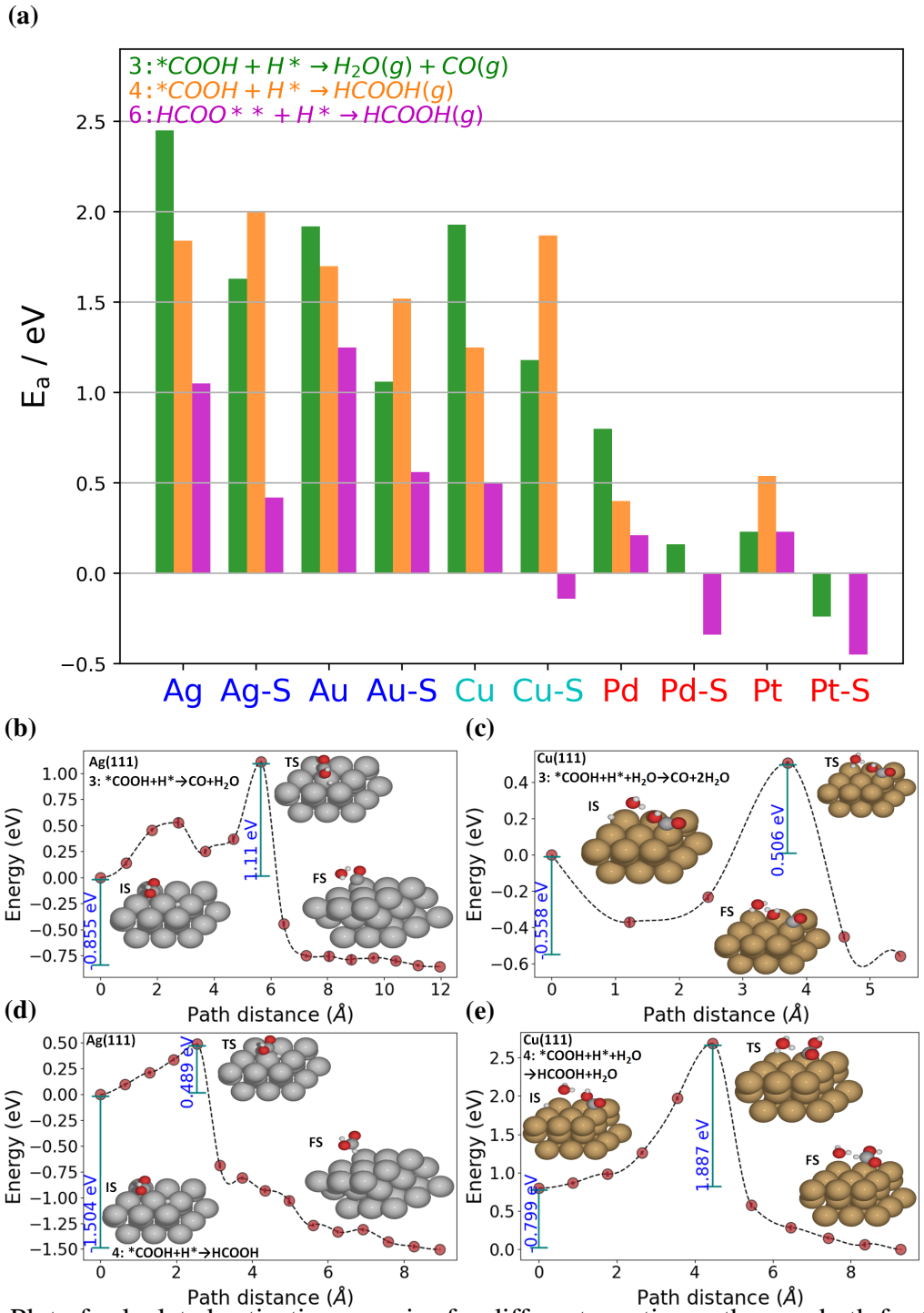

Figure 5: Plot of calculated activation energies for different reaction pathways, both for the direct pathway where *H comes from the catalyst surface, and via the water-assisted proton-shuttled ('-S') pathway. **(a)** Reaction barrier energy for pathways 3, 4, 6, and 7. Metal catalysts are colored in accordance with their major product selectivity as shown in Fig. 1a. **(b)** Transition state pathway for pathways 3 and 4, without (**left**) and with (**right**) water-assisted proton-shuttling.

stability and ease of formation for HCOO** compared to *COOH, it is possible that CO formation occurs via a different mechanism compared to HCOOH formation. Fig. 5a shows the reaction barriers for the three different pathways for CO vs. HCOOH formation, Eq. 3 (green), Eq. 4 (orange), and Eq. 6 (purple). Eq. 5 does not occur, as the intermediate HCOO** first rearranges itself to *COOH via an energetically unviable step, and then follows pathway 3 (see SI section "Additional Transition State Results"). The barriers are via direct protonation by *H, and via water-assisted H-shuttled hydrogenation ('-S-' in the plot) as described by Nie et al.[45,46] Fig. 5b shows reaction pathways for the direct protonation mechanism (left) and the water-assisted mechanism (right), along with atomic-scale insets of the initial state (IS), transitition state (TS), and final state (FS). We observe that for the direct protonation results, HCOOH formation has a lower barrier than CO formation on CO (orange bar is smaller than green bar) from monodentate *COOH, with HCOOH formation from HCOO** (purple bar) being even lower. However, if using the water-assisted H-shuttled hydrogenation for *COOH to CO formation (pathway 3 (see SI section "*Additional Transition State Results*"), but keeping the non-water-assisted pathway results for HCOOH formation (see 5), pathway 3 is the lowest-energy pathway on Au by rougly 0.2 eV, and is the lowest pathway from *COOH for Ag. This would explain Ag and Au's predilection for making CO using simulations, in agreement with experimental results. This has to our knowledge not been shown directly before with DFT calculations. However, this only gives us one piece of the puzzle, since HCOO** is still more stable than *COOH on Ag and Au (see Fig. 1b), and also forms more readily from CO_2 (see SI Section "*Direct Reaction Pathway Results*"). As such, an explanation of how monodentate *COOH or HCOO* occurs on the Ag/Au surface could be the missing link. Note that we also attempted the water-assisted shuttling mechanism for Pb and other HCOOH-producing metals. This pathway was however found unviable under all permutations and conformations, as the distance between the surface, the *H, and the H_2O was too large for the mechanism to occur, because of the adsorption energies of the species and the larger lattice constant of HCOOH-producing metals (see Fig. 4). Instead, *H adsorps directly to the intermediate. As such, we believe this Tafel mechanism to be the pathway for HCOOH formation, as opposed to

the Heyrovsky mechanism for CO formation, as also hypothesized by Morrison et al.[30]

In short, if we assume that *COOH makes CO (and possibly HCOOH) via the water-assisted shuttling mechanism, but that HCOO** makes HCOOH via the Tafel mechanism, then CO formation has the lowest activation barrier on Au and Ag. Even if we assume that HCOO** to HCOOH also occurs via water shuttling, that still makes *COOH more likely to make CO than HCOOH. Meaning, if there is monodentate *COOH (or HCOO*) on the surface, it makes CO, in agreement with experiments. This is what our coverage analysis means to show.

4.2 Monodentate *COOH/HCOO* on Surface on Surface at High Coverage

In catalysis, DFT with a single adsorbate on catalyst surfaces are usually used as a descriptor to describe the energetic trends of the catalytic system. Although this assumption has generally proven solid,[2] the electrochemical CO_2 reduction reaction, with its manifold and complex reaction pathways,[1,7,8] might benefit from considering how multiple different adsorbates on the surface interact with each other.[29,30,35,47]

For this reason, we decided to perform a coverage analysis of our investigated adsorbates, going from 1/9ths to 1 ML coverage on a 3x3x3 metal atom surface. While recent studies have looked at higher coverages of adsorbates, these studies only increase the coverage of a single adsorbate.[30,32] Here, we mix together our 5 different adsorbates for all possible combinations and coverages, leading to more than 300 adsorbate combinations on the surface. The idea is that at high coverages, with different adsorbate-adsorbate interactions, different adsorbate combinations might be the most stable. Ag and Au might be shown to have monodentate adsorbates on the surface, and thus be shown capable of making CO as discussed in the previous section. For more details, see the "Methodology" section in the SI.

Fig. 6 shows the Boltzmann-averaged coverage of adsorbates on Ag (Fig. 6a) and Au (Fig. 6b) as a function of RHE potential. For atomic visualizations of the most stable adsorbate combination at potentials 0.0, -0.6, and -1.2 V vs. RHE, see the SI section "*Additional Coverage Analysis Results*". At high coverages of *H with *COOH/HCOO**, reactions can happen due to instability

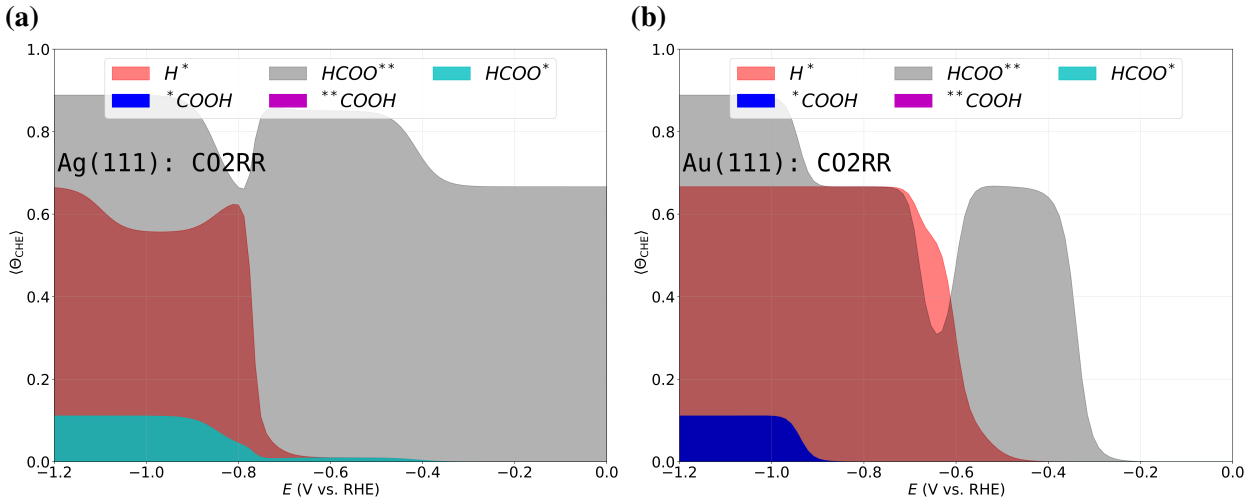

Figure 6: (**a-b**) Interface phase diagrams calculated by Boltzmann weighting of the energies obtained from the CHE scheme to give the most stable adsorbate configurations as a function of potential. (**a**) Ag, (**b**) Au. For visualizations of the different adsorbate types in the legend, see Fig. 2. For atomic visualizations of the most stable adsorbate combination at potentials 0.0, -0.6, and -1.2 V vs. RHE, see the SI section "*Additional Coverage Analysis Results*".

of the adsorbate combination, with it making CO, HCOOH, and/or H_2CO_3. As the adsorbates are no longer on the surface, these results are not usable for this analysis and only results up to 2/3 ML *H coverage are shown here. Including higher *H coverage does not change the trends.

For the Ag interface phase diagram (Fig. 6a), we observe that at low potential, there is only HCOO** at the surface, but as the potential increases, we also start to get *H and monodentate HCOO*. Au (Fig. 6b) shows the same trend, only with *COOH instead of monodentate HCOO*. In other words, Ag and Au can make CO, in qualitative agreement with experiments, due to the presence of monodentate intermediates on the surface. This is to our knowledge the first DFT calculation setup that contains CO-producing intermediates as the most stable phase on Ag and Au. While the phase diagrams for Ag and Au reproduce experimental trends, at least qualitatively, for the method to be robust it also needs to work for the other major product types in Fig. 1a. For this reason, we did the same analysis on other metal calysts (see SI section "*Additional Coverage Analysis Results*"). As an example, Pb (Fig. S18c) shows the expected result of full bidentate HCOO** coverage, barring a short blip of monodentate HCOO* around -0.6 V vs. RHE. As bidentate HCOO** exclusively produces HCOOH, this is also in agreement with the metal's actual

product selectivity. Another thing to note is that the potential at which CO_2RR begins according to these calculations, i.e. where there is both *H and either monodentate species for CO formation, agrees qualitatively with the onset potentials calculated by Hori et al.[23] For example, Hori et al. finds the onset potentials for Au and Ag to be -0.74 and -0.97 V vs. RHE, respectively, which aligns roughly with the values found in Figures 6a-b.

These results show the presence of CO-producing intermediates on the surface of Ag and Au, but raises new questions. Because there is still far more bidentate HCOO** on the surface than there are monodentate CO-producing intermediates. So why does HCOO** on Ag and Au not make HCOOH? A possible hypothesis is that the bidentate structure on the surface is not actually HCOO**, but a different bidentate adsorbate. It could be carbonate (CO_3^{2-}) or bicarbonate (HCO_3^-), which is inert for CO_2RR and, and would explain the product selectivity of Ag and Au. This possibility seems supported by literature.[29,36,48–54] However, it can be difficult to determine exactly what the bidentate structure on the surface is; some authors have found bidentate peak frequencies on Ag or Au and assigned it to HCOO**,[29] while others get similar peak frequencies and assign it to (bi)carbonate.[50,54] However, we would expect (bi)carbonate to become unstable and desorb from the surface at negative potentials, making it unlikely for there to be a high coverage of it at CO_2RR potentials.

5 Conclusion and Outlook

We here briefly restate our most important novel findings, and what the still existing questions and limitations are for explaining CO_2R product selectivity using simulations:

- By doing PCA on our many descriptors, we are able to properly separate and classify the CO_2RR metal catalysts according to their major product distribution.
- The descriptors *H, *CO, and lLC also classify the metal catalyst, showing that CO_2RR product selectivity can be explained using only a few descriptors, and directly connecting

physical descriptors to CO vs. HCOOH product selectivity as dependent on the catalyst surface.

- By considering the water-assisted shuttling mechanism, we have shown that CO formation has the lowest reaction barrier on Au and Ag (or at least that monodentate intermediates preferentially make CO). This was previously a discrepancy between simulations and experiments, as the HCOOH formation pathway seemed to be lower in energy.[11,29]

- By considering high coverage of mixed adsorbates, we have shown that both Ag and Au have monodentate adsorbates on the surface at CO_2RR potentials, showing their ability to make CO from these intermediates. This was previously a discrepancy between simulations and experiments, as the bidentate, HCOOH-producing HCOO** intermediate was shown to be more stable than the *COOH intermediate.

- We still have not fully shown why CO would be the main product for Au and Ag, due to the proliferation of bidentate adsorbate on the surface. By investigating the possibility that the bidentate can rearrange to *COOH, or be inert (bi)carbonate instead of HCOO**, however, we have laid the groundwork for further investigation into the CO_2R product distribution.

In conclusion, explaining the difference between CO- and HCOOH-producing metal catalysts for CO_2RR, along with why Ag and Au primarily produce CO, is one of the big gaps in our understanding of the reaction. With this approach, we now have qualitative agreement between simulations and experimental work regarding CO_2R selectivity. However, there are still open questions regarding the role and species of the bidentate adsorbate on CO-producing metals, and whether it is a spectator or something else. As such, this may not be the complete solution to the question of CO vs. HCOOH selectivity for CO_2RR, but we believe that it is a valid, empirically based possible explanation that answers many of the questions. Further work would likely include considering how best to falsify this theory, and testing it thus. We should also note that even including water-assisted shuttling and the many different features used for the PCA, our analysis is in no

way all-encompassing. As an example, our analysis does not include the effect of cations, despite previous work having shown their their importance for CO_2RR.[55]

6 Computational Approach

All calculations were performed using DFT,[56] utilizing ASE version 3.19.0, and GPAW version 19.8.1.[57,58] Calculations were done at the Generalized Gradient Approximation (GGA) level of theory, utilizing the plane-wave (PW) mode,[59] with the BEEF-vdW functional.[60] We use a k-point sampling appropriate for the specific structure, a plane wave cutoff of $E_{cut} = 400$ eV, and a vacuum of minimum 10 Å. All structures are relaxed to a force below 0.05 eV/Å. The slabs, unless otherwise noted, are FCC(111) 3x3x3 unit cells with fixed bottom layers. Spin-polarization was applied for Fe, Co, and Ni structures. The binding energies and activation energies were calculated relative to the gas-phase reference. The transition states were calculated using the Nudged Elastic Band (NEB) method,[61] using the ML-NEB implementation as part of the CatLearn package.[62,63]

Acknowledgement

O.C. and J.R. acknowledge the Danish National Research Foundation Centers of Excellence, the Center for High Entropy Alloy Catalysis (Project DNRF149).

The authors declare no conflicts of interest.

Supporting Information Available

Structures, energies, and the plotting methods used in this article can be found at (http://nano.ku.dk/english/research/theoretical-electrocatalysis/katladb/).

References

(1) Nitopi, S.; Bertheussen, E.; Scott, S. B.; Liu, X.; Engstfeld, A. K.; Horch, S.; Seger, B.; Stephens, I. E.; Chan, K.; Hahn, C., et al. Progress and perspectives of electrochemical CO_2 reduction on copper in aqueous electrolyte. *Chemical reviews* **2019**, *119*, 7610–7672.

(2) Seh, Z. W.; Kibsgaard, J.; Dickens, C. F.; Chorkendorff, I.; Nørskov, J. K.; Jaramillo, T. F. Combining theory and experiment in electrocatalysis: Insights into materials design. *Science* **2017**, *355*.

(3) De Luna, P.; Hahn, C.; Higgins, D.; Jaffer, S. A.; Jaramillo, T. F.; Sargent, E. H. What would it take for renewably powered electrosynthesis to displace petrochemical processes? *Science* **2019**, *364*.

(4) Chu, S.; Cui, Y.; Liu, N. The path towards sustainable energy. *Nature Materials* **2016**, *16*, 16.

(5) Hepburn, C.; Adlen, E.; Beddington, J.; Carter, E. A.; Fuss, S.; Mac Dowell, N.; Minx, J. C.; Smith, P.; Williams, C. K. The technological and economic prospects for CO_2 utilization and removal. *Nature* **2019**, *575*, 87–97.

(6) Pörtner, H.-O.; Roberts, D. C.; Masson-Delmotte, V.; Zhai, P.; Tignor, M.; Poloczanska, E.; Mintenbeck, K.; Nicolai, M.; Okem, A.; Petzold, J., et al. IPCC special report on the ocean and cryosphere in a changing climate. *IPCC Intergovernmental Panel on Climate Change: Geneva, Switzerland* **2019**, *1*.

(7) Ulissi, Z. W.; Medford, A. J.; Bligaard, T.; Nørskov, J. K. To address surface reaction network complexity using scaling relations machine learning and DFT calculations. *Nature communications* **2017**, *8*, 1–7.

(8) Stephens, I. E.; Chan, K.; Bagger, A.; Boettcher, S. W.; Bonin, J.; Boutin, E.; Buckley, A. K.; Buonsanti, R.; Cave, E. R.; Chang, X., et al. 2022 roadmap on low temperature electrochemical CO_2 reduction. *Journal of Physics: Energy* **2022**, *4*, 042003.

(9) Hori, Y.; Murata, A.; Takahashi, R. Formation of hydrocarbons in the electrochemical reduction of carbon dioxide at a copper electrode in aqueous solution. *Journal of the Chemical Society, Faraday Transactions 1: Physical Chemistry in Condensed Phases* **1989**, *85*, 2309–2326.

(10) Kortlever, R.; Shen, J.; Schouten, K. J. P.; Calle-Vallejo, F.; Koper, M. T. Catalysts and reaction pathways for the electrochemical reduction of carbon dioxide. *The journal of physical chemistry letters* **2015**, *6*, 4073–4082.

(11) Yoo, J. S.; Christensen, R.; Vegge, T.; Nørskov, J. K.; Studt, F. Theoretical insight into the trends that guide the electrochemical reduction of carbon dioxide to formic acid. *ChemSusChem* **2016**, *9*, 358–363.

(12) Nørskov, J. K.; Bligaard, T.; Logadottir, A.; Kitchin, J.; Chen, J. G.; Pandelov, S.; Stimming, U. Trends in the exchange current for hydrogen evolution. *Journal of The Electrochemical Society* **2005**, *152*, J23.

(13) Chen, Y.; Li, C. W.; Kanan, M. W. Aqueous CO_2 reduction at very low overpotential on oxide-derived Au nanoparticles. *Journal of the American Chemical Society* **2012**, *134*, 19969–19972.

(14) Mistry, H.; Reske, R.; Zeng, Z.; Zhao, Z.-J.; Greeley, J.; Strasser, P.; Cuenya, B. R. Exceptional size-dependent activity enhancement in the electroreduction of CO_2 over Au nanoparticles. *Journal of the American Chemical Society* **2014**, *136*, 16473–16476.

(15) Nguyen, D. L. T.; Jee, M. S.; Won, D. H.; Jung, H.; Oh, H.-S.; Min, B. K.; Hwang, Y. J. Selective CO_2 reduction on zinc electrocatalyst: the effect of zinc oxidation state induced by pretreatment environment. *ACS Sustainable Chemistry & Engineering* **2017**, *5*, 11377–11386.

(16) Lu, Q.; Rosen, J.; Jiao, F. Nanostructured metallic electrocatalysts for carbon dioxide reduction. *ChemCatChem* **2015**, *7*, 38–47.

(17) Mistry, H.; Choi, Y.-W.; Bagger, A.; Scholten, F.; Bonifacio, C. S.; Sinev, I.; Divins, N. J.; Zegkinoglou, I.; Jeon, H. S.; Kisslinger, K., et al. Enhanced carbon dioxide electroreduction to carbon monoxide over defect-rich plasma-activated silver catalysts. *Angewandte Chemie* **2017**, *129*, 11552–11556.

(18) Ma, M.; Trześniewski, B. J.; Xie, J.; Smith, W. A. Selective and efficient reduction of carbon dioxide to carbon monoxide on oxide-derived nanostructured silver electrocatalysts. *Angewandte Chemie* **2016**, *128*, 9900–9904.

(19) Chen, Y.; Kanan, M. W. Tin oxide dependence of the CO_2 reduction efficiency on tin electrodes and enhanced activity for tin/tin oxide thin-film catalysts. *Journal of the American Chemical Society* **2012**, *134*, 1986–1989.

(20) Baruch, M. F.; Pander III, J. E.; White, J. L.; Bocarsly, A. B. Mechanistic insights into the reduction of CO_2 on tin electrodes using in situ ATR-IR spectroscopy. *Acs Catalysis* **2015**, *5*, 3148–3156.

(21) Luc, W.; Collins, C.; Wang, S.; Xin, H.; He, K.; Kang, Y.; Jiao, F. Ag–Sn bimetallic catalyst with a core–shell structure for CO_2 reduction. *Journal of the American chemical society* **2017**, *139*, 1885–1893.

(22) Hori, Y.; Kikuchi, K.; Murata, A.; Suzuki, S. Production of methane and ethylene in electrochemical reduction of carbon dioxide at copper electrode in aqueous hydrogencarbonate solution. *Chemistry Letters* **1986**, *15*, 897–898.

(23) Hori, Y.; Wakebe, H.; Tsukamoto, T.; Koga, O. Electrocatalytic process of CO selectivity in electrochemical reduction of CO_2 at metal electrodes in aqueous media. *Electrochimica Acta* **1994**, *39*, 1833–1839.

(24) Li, C. W.; Ciston, J.; Kanan, M. W. Electroreduction of carbon monoxide to liquid fuel on oxide-derived nanocrystalline copper. *Nature* **2014**, *508*, 504–507.

(25) Verdaguer-Casadevall, A.; Li, C. W.; Johansson, T. P.; Scott, S. B.; McKeown, J. T.; Kumar, M.; Stephens, I. E.; Kanan, M. W.; Chorkendorff, I. Probing the active surface sites for CO reduction on oxide-derived copper electrocatalysts. *Journal of the American Chemical Society* **2015**, *137*, 9808–9811.

(26) Mistry, H.; Varela, A. S.; Bonifacio, C. S.; Zegkinoglou, I.; Sinev, I.; Choi, Y.-W.; Kisslinger, K.; Stach, E. A.; Yang, J. C.; Strasser, P., et al. Highly selective plasma-activated copper catalysts for carbon dioxide reduction to ethylene. *Nature communications* **2016**, *7*, 1–9.

(27) Schouten, K. J. P.; Qin, Z.; Peérez Gallent, E.; Koper, M. T. Two pathways for the formation of ethylene in CO reduction on single-crystal copper electrodes. *Journal of the American Chemical Society* **2012**, *134*, 9864–9867.

(28) Bagger, A.; Ju, W.; Varela, A. S.; Strasser, P.; Rossmeisl, J. Electrochemical CO_2 reduction: a classification problem. *ChemPhysChem* **2017**, *18*, 3266–3273.

(29) Bohra, D.; Ledezma-Yanez, I.; Li, G.; de Jong, W.; Pidko, E. A.; Smith, W. A. Lateral adsorbate interactions inhibit HCOO- while promoting CO selectivity for CO_2 electrocatalysis on silver. *Angewandte Chemie* **2019**, *131*, 1359–1363.

(30) Morrison, A. R.; Ramdin, M.; Van Der Broeke, L. J.; De Jong, W.; Vlugt, T. J.; Kortlever, R. Surface Coverage as an Important Parameter for Predicting Selectivity Trends in Electrochemical CO_2 Reduction. *The Journal of Physical Chemistry C* **2022**, *126*, 11927–11936.

(31) Shan, W.; Liu, R.; Zhao, H.; Liu, J. Bicarbonate Rebalances the* COOH/* OCO–Dual Pathways in CO_2 Electrocatalytic Reduction: In Situ Surface-Enhanced Raman Spectroscopic Evidence. *The Journal of Physical Chemistry Letters* **2022**, *13*, 7296–7305.

(32) Chen, X.; Granda-Marulanda, L. P.; McCrum, I. T.; Koper, M. T. How palladium inhibits CO poisoning during electrocatalytic formic acid oxidation and carbon dioxide reduction. *Nature Communications* **2022**, *13*, 38.

(33) Kim, C.; Bui, J. C.; Luo, X.; Cooper, J. K.; Kusoglu, A.; Weber, A. Z.; Bell, A. T. Tailored catalyst microenvironments for CO_2 electroreduction to multicarbon products on copper using bilayer ionomer coatings. *Nature Energy* **2021**, *6*, 1026–1034.

(34) Seifitokaldani, A.; Gabardo, C. M.; Burdyny, T.; Dinh, C.-T.; Edwards, J. P.; Kibria, M. G.; Bushuyev, O. S.; Kelley, S. O.; Sinton, D.; Sargent, E. H. Hydronium-induced switching between CO_2 electroreduction pathways. *Journal of the American Chemical Society* **2018**, *140*, 3833–3837.

(35) Herrero, E.; Feliu, J. M. Understanding formic acid oxidation mechanism on platinum single crystal electrodes. *Current Opinion in Electrochemistry* **2018**, *9*, 145–150.

(36) Katayama, Y.; Nattino, F.; Giordano, L.; Hwang, J.; Rao, R. R.; Andreussi, O.; Marzari, N.; Shao-Horn, Y. An in situ surface-enhanced infrared absorption spectroscopy study of electrochemical CO_2 reduction: selectivity dependence on surface C-bound and O-bound reaction intermediates. *The Journal of Physical Chemistry C* **2018**, *123*, 5951–5963.

(37) Feaster, J. T.; Shi, C.; Cave, E. R.; Hatsukade, T.; Abram, D. N.; Kuhl, K. P.; Hahn, C.; Nørskov, J. K.; Jaramillo, T. F. Understanding selectivity for the electrochemical reduction of carbon dioxide to formic acid and carbon monoxide on metal electrodes. *Acs Catalysis* **2017**, *7*, 4822–4827.

(38) Deng, W.; Zhang, P.; Seger, B.; Gong, J. Unraveling the rate-limiting step of two-electron transfer electrochemical reduction of carbon dioxide. *Nature communications* **2022**, *13*, 1–9.

(39) Tang, M. T.; Peng, H.; Lamoureux, P. S.; Bajdich, M.; Abild-Pedersen, F. From electricity to fuels: descriptors for C1 selectivity in electrochemical CO_2 reduction. *Applied Catalysis B: Environmental* **2020**, *279*, 119384.

(40) Hussain, J.; Joénsson, H.; Skuélason, E. Calculations of product selectivity in electrochemical CO_2 reduction. *Acs Catalysis* **2018**, *8*, 5240–5249.

(41) Calle-Vallejo, F.; Koper, M. T. Theoretical considerations on the electroreduction of CO to C_2 species on Cu (100) electrodes. *Angewandte Chemie* **2013**, *125*, 7423–7426.

(42) Montoya, J. H.; Shi, C.; Chan, K.; Nørskov, J. K. Theoretical insights into a CO dimerization mechanism in CO_2 electroreduction. *The journal of physical chemistry letters* **2015**, *6*, 2032–2037.

(43) Bro, R.; Smilde, A. K. Principal component analysis. *Analytical methods* **2014**, *6*, 2812–2831.

(44) Yang, S.; An, H.; Arnouts, S.; Wang, H.; Yu, X.; de Ruiter, J.; Bals, S.; Altantzis, T.; Weckhuysen, B. M.; van der Stam, W. Halide-guided active site exposure in bismuth electrocatalysts for selective CO2 conversion into formic acid. *Nature Catalysis* **2023**, 1–11.

(45) Nie, X.; Esopi, M. R.; Janik, M. J.; Asthagiri, A. Selectivity of CO_2 reduction on copper electrodes: the role of the kinetics of elementary steps. *Angewandte Chemie* **2013**, *125*, 2519–2522.

(46) Nie, X.; Luo, W.; Janik, M. J.; Asthagiri, A. Reaction mechanisms of CO_2 electrochemical reduction on Cu (1 1 1) determined with density functional theory. *Journal of catalysis* **2014**, *312*, 108–122.

(47) Bagger, A.; Arnarson, L.; Hansen, M. H.; Spohr, E.; Rossmeisl, J. Electrochemical CO reduction: A property of the electrochemical interface. *Journal of the American Chemical Society* **2019**, *141*, 1506–1514.

(48) Amirbeigiarab, R.; Bagger, A.; Tian, J.; Rossmeisl, J.; Magnussen, O. M. Structure of the (bi) carbonate adlayer on Cu (100) electrodes. *Angewandte Chemie International Edition* **2022**, *61*, e202211360.

(49) Ma, W.; He, X.; Wang, W.; Xie, S.; Zhang, Q.; Wang, Y. Electrocatalytic reduction of CO_2

and CO to multi-carbon compounds over Cu-based catalysts. *Chemical Society Reviews* **2021**, *50*, 12897–12914.

(50) Martínez-Hincapié, R.; Rodes, A.; Climent, V.; Feliu, J. M. Surface charge and interfacial acid-base properties: pKa, 2 of carbon dioxide at Pt (110)/perchloric acid solution interfaces. *Electrochimica Acta* **2021**, *388*, 138639.

(51) Jouny, M.; Luc, W.; Jiao, F. High-rate electroreduction of carbon monoxide to multi-carbon products. *Nature Catalysis* **2018**, *1*, 748–755.

(52) Verma, S.; Hamasaki, Y.; Kim, C.; Huang, W.; Lu, S.; Jhong, H.-R. M.; Gewirth, A. A.; Fujigaya, T.; Nakashima, N.; Kenis, P. J. Insights into the low overpotential electroreduction of CO_2 to CO on a supported gold catalyst in an alkaline flow electrolyzer. *ACS Energy Letters* **2017**, *3*, 193–198.

(53) Kai, S.; Chaozhi, W.; Guangzhi, X. Surface enhanced Raman spectra of carbonate, hydrocarbonate, and substituted acetic acids on silver hydrosols. *Spectrochimica Acta Part A: Molecular Spectroscopy* **1989**, *45*, 1029–1032.

(54) Arihara, K.; Kitamura, F.; Ohsaka, T.; Tokuda, K. Characterization of the adsorption state of carbonate ions at the Au (111) electrode surface using in situ IRAS. *Journal of Electroanalytical Chemistry* **2001**, *510*, 128–135.

(55) Monteiro, M. C.; Dattila, F.; Hagedoorn, B.; García-Muelas, R.; López, N.; Koper, M. T. Absence of CO2 electroreduction on copper, gold and silver electrodes without metal cations in solution. *Nature Catalysis* **2021**, *4*, 654–662.

(56) Hohenberg, P.; Kohn, W. Inhomogeneous electron gas. *Physical review* **1964**, *136*, B864.

(57) Larsen, A. H.; Mortensen, J. J.; Blomqvist, J.; Castelli, I. E.; Christensen, R.; Dułak, M.; Friis, J.; Groves, M. N.; Hammer, B.; Hargus, C., et al. The atomic simulation environ-

ment—a Python library for working with atoms. *Journal of Physics: Condensed Matter* **2017**, *29*, 273002.

(58) Enkovaara, J.; Rostgaard, C.; Mortensen, J. J.; Chen, J.; Dułak, M.; Ferrighi, L.; Gavnholt, J.; Glinsvad, C.; Haikola, V.; Hansen, H., et al. Electronic structure calculations with GPAW: a real-space implementation of the projector augmented-wave method. *Journal of Physics: Condensed Matter* **2010**, *22*, 253202.

(59) Troullier, N.; Martins, J. L. Efficient pseudopotentials for plane-wave calculations. *Physical review B* **1991**, *43*, 1993.

(60) Wellendorff, J.; Lundgaard, K. T.; Møgelhøj, A.; Petzold, V.; Landis, D. D.; Nørskov, J. K.; Bligaard, T.; Jacobsen, K. W. Density functionals for surface science: Exchange-correlation model development with Bayesian error estimation. *Physical Review B* **2012**, *85*, 235149.

(61) Jónsson, H.; Mills, G.; Jacobsen, K. W. Nudged elastic band method for finding minimum energy paths of transitions. **1998**,

(62) Hansen, M. H.; Torres, J. A. G.; Jennings, P. C.; Wang, Z.; Boes, J. R.; Mamun, O. G.; Bligaard, T. An atomistic machine learning package for surface science and catalysis. *arXiv preprint arXiv:1904.00904* **2019**,

(63) Torres, J. A. G.; Jennings, P. C.; Hansen, M. H.; Boes, J. R.; Bligaard, T. Low-scaling algorithm for nudged elastic band calculations using a surrogate machine learning model. *Physical review letters* **2019**, *122*, 156001.